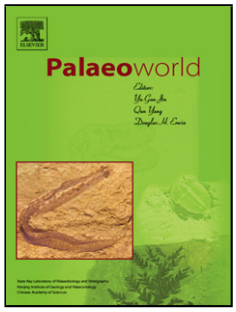


Title: Palaeoenvironmental changes recorded in the palynology and palynofacies of a Late Permian Marker Mudstone (Galilee Basin, Australia)

Authors: Alexander Wheeler, Nikola Van de Wetering, Joan Esterle, Annette E. Götz

PII: S1871-174X(18)30080-5
DOI: https://doi.org/10.1016/j.palwor.2018.10.005
Reference: PALWOR 476

To appear in: *Palaeoworld*

Received date: 25 May 2018
Revised date: 11 October 2018
Accepted date: 26 October 2018

Please cite this article as: Wheeler, Alexander, Van de Wetering, Nikola, Esterle, Joan, Götz, Annette E., Palaeoenvironmental changes recorded in the palynology and palynofacies of a Late Permian Marker Mudstone (Galilee Basin, Australia).Palaeoworld https://doi.org/10.1016/j.palwor.2018.10.005

# Palaeoenvironmental changes recorded in the palynology and palynofacies of a Late Permian Marker Mudstone (Galilee Basin, Australia)

Alexander Wheeler [a *] a.wheeler@uq.edu.au , Nikola Van de Wetering [a], Joan Esterle [a], Annette E. Götz [b, c]

[a] School of Earth and Environmental Sciences, The University of Queensland, St. Lucia QLD 4072, Australia

[b] School of Earth and Environmental Sciences, University of Portsmouth, Portsmouth, PO1 3QL, United Kingdom

[c] Kazan Federal University, 18 Kremlyovskaya Street, Kazan 420008, Republic of Tatarstan, Russian Federation

[*] **Corresponding author**.

## Abstract

Reconstructing the terrestrial palaeoenvironment during the end-Permian is made challenging by widespread erosion and ecosystem destruction. High-resolution sampling for palynofacies and palynology in sections that preserve the boundary interval allows for detailed examination of the drastic environmental changes that characterize the Permian–Triassic mass extinction. In the Bowen and Galilee basins in eastern Australia, this environmental perturbation is recorded within a Marker Mudstone that occurs above the uppermost Permian coal seams. The Marker Mudstone is used as a stratigraphic reference level at many localities, but has previously only been studied at a single locality in the Bowen Basin. In the present study, borehole Tambo 1-1A drilled in the Galilee Basin was selected to clarify whether this black, organic-rich mudstone marks a marine transgression, and to examine potential indicators of the end-Permian mass extinction. A total of 22 samples were taken from the mudstone unit, and from the over- and underlying strata and processed for palynology, palynofacies, and carbon isotope analysis.

Biostratigraphic data indicate that the Marker Mudstone itself covers the uppermost part of unit APP5, with the first index taxa of unit APP6 floras occurring in samples less than 80 cm above this interval. This can be correlated with several other localities in the Bowen and Sydney basins where this shift occurs just above the

uppermost Permian coal seam. Palynofacies data agree with previous interpretations of a southwards prograding delta that subsides as base level rises to form an extensive waterbody in which the Marker Mudstone was deposited. A change from translucent phytoclast-dominated to opaque phytoclast-dominated palynofacies within the Marker Mudstone suggests a shift to more oxic conditions in the water column, while base level begins to fluctuate, or increased terrestrial input from fluvial systems as the hinterland rises. Algal bodies resembling *Botryococcus* are found in the strata above the Marker Mudstone, but differ in morphology from the algal bodies found in the deltaic facies below. The presence of acanthomorph acritarchs in the Marker Mudstone and in the overlying Rewan Formation may indicate marine influence. Forms resembling fungal spores are present, but they do not show a "spike" as seen in other P–T boundary localities.

The relative position of unit APP6 to the P–T boundary itself remains unclear. APP6 assemblages are dominated by simple acavate trilete and cavate trilete spores, which suggests stressed environment dominated by ferns and lycopods. The presence of degraded phytoclasts towards the top of the Marker Mudstone may also be used to suggest a mass-extinction interval. They may also be indicative of shifting local palaeoenvironmental changes, an interpretation that is supported by the low magnitude negative excursion of the $\delta^{13}C$ isotope values within the Marker Mudstone. More datasets from the Bowen and Galilee basins will be essential to decoupling these signals.

**Keywords:** Palynology; Palynofacies; Carbon isotopes; Palaeoenvironment; Permian–Triassic boundary; Galilee Basin

## 1. Introduction

Deciphering patterns and processes of environmental change across the Permian–Triassic boundary in the terrestrial basins of Gondwana has long been a challenge (e.g., de Wit et al., 2002; Gastaldo et al., 2009; Smith and Botha-Brink, 2014). In eastern Australia, integrated palynological and geochronological studies have shown great utility for dating and correlating the late Permian deposits (Smith and Mantle, 2013; Laurie et al., 2016). Potential sections in the Galilee Basin in particular have remained understudied when compared to those of other eastern Australian basins such as the Bowen, Gunnedah and Sydney basins (Figs. 1, 2). The Galilee Basin is

only recently beginning to receive attention for its economic resource potential (Hansen and Uroda, 2018; I'Anson et al., 2018), but it may also contain valuable climatic and environmental records of the late Palaeozoic that have yet to be exploited. Of special importance is that the Galilee Basin was situated relatively far away from the tectonic activity in the New England Orogen and that it captures a terrestrial-marine transition from the north to the south and across the Springsure Shelf, which allows for detailed study of various depositional environments. In many parts of the Bowen and Galilee basins, a regional disconformity to low-angle unconformity at the base of the Rewan Formation represents an erosional contact that probably removed the Permian–Triassic boundary itself within the basins (Brakel et al., 2009; Sliwa et al., 2017). Recent systematic correlation, however, revealed that where this unconformity is not observed, there remains a laterally continuous mudstone interval that is deposited above the last coal deposits of the Permian (Sliwa et al., 2017). This mudstone is recognised as a prominent gamma spike in wireline logs, and has been termed the "Marker Mudstone" due to its consistency and utilization for basin-wide correlation. Michaelsen et al. (2000) and Michaelsen (2002) interpreted the Marker Mudstone as a lake deposit that developed above the peat deposits immediately preceding the P–T boundary; however, the precise nature and origin of this mudstone remain unknown. The aims of this study are: 1) to place the Marker Mudstone within a biostratigraphic context, 2) to develop a palaeoenvironmental interpretation based on palynology and palynofacies, and 3) to determine if palynological markers (e.g., fungal spike, lycopsid spike) reported from other localities exposing the Permian–Triassic boundary are present.

## 2. Geological setting

The Galilee Basin is an intracratonic basin that covers an area of around 247,000 $km^2$ in central Queensland (Fig. 1) (Allen and Fielding, 2007). The sediment infill occurred during two major phases of deposition from the Pennsylvanian (late Carboniferous) to the Cisuralian (early Permian) and from the Lopingian (late Permian) to the Middle Triassic, separated by a mid-Permian depositional hiatus. This hiatus is attributed to reduced rates of deposition rather than to erosion, as there is little evidence of an erosional unconformity (Van Heeswijck, 2010; Phillips et al., 2018). The basement comprises the Devonian–Carboniferous Drummond Basin in the east, the Thomson Orogen in the centre, and Precambrian cratonic rocks in the west.

Large areas of the basin are overlain by the Jurassic–Cretaceous deposits of the Eromanga Basin (Fig. 2). The Galilee and Bowen basins are separated by the Nebine Ridge on a structural high called the Springsure Shelf. The Galilee Basin is separated from the Cooper Basin by the Canaway Ridge in the south-west of the basin.

The complex nature of the late Permian deposits has long made lithostratigraphic and sequence stratigraphic correlation a challenge. Allen and Fielding (2007) worked on a sequence stratigraphic correlation of the low-accommodation setting of the Betts Creek Beds relative to the high accommodation setting of the Denison Trough in the Bowen Basin, and identified second (10–100 Ma) and third-order (1–10 Ma) sequences in outcrops and well logs. The lithostratigraphic correlation has been reinterpreted by different authors in different regions within the basin (Fig. 3) as summarised by Phillips et al. (2017). Large-scale correlations across the Galilee Basin recently allowed the identification of the Marker Mudstone along the eastern margin of the basin and in the borehole GSQ Tambo 1-1A (Phillips et al., 2017).

**Permian–Triassic boundary**

The Permian–Triassic boundary is formally defined at the Global Boundary Stratotype Section and Point (GSSP) in the marine Meishan Beds in China by the first appearance of the conodont *Hindeodus parvus*. This horizon is located several centimetres above the mass extinction interval (Yin et al., 2001). The extinction is estimated to have affected between 80% and 95% of marine species, including trilobites, fusulinid foraminifera and various groups of echinoderms and brachiopods (Benton and Twitchett, 2003). In terrestrial basins, a number of proxies are useful in placing the boundary. One of the most widely recognised indicators of the boundary is a negative carbon isotopic excursion (Retallack and Krull, 2006). This excursion is thought to be related to an increase in global $CO_2$ from increased volcanic activity at the end of the Permian (Svensen et al., 2009). In terms of palynological indicators, several authors (Eshet et al., 1995; Visscher et al., 1996; Steiner et al., 2003; Bercovici and Vajda, 2016) have recognised a spike in the abundance of fungal remains such as *Reduviasporonites chalastus*, though it has been suggested that this species may have an algal affinity (Foster et al., 2002) or even be a result of recent contamination (Hochuli, 2016). Spina et al. (2015) suggest that *R. chalastus* is a chlorophycean algae with a strong affinity for brackish to hypersaline water, and cannot be used as a consistent temporal marker.

In eastern Australia, the boundary has historically been placed at the top of the last Permian coal deposits (Laurie et al., 2016). In the Bowen Basin, this would correspond to the interface of the Bandanna Formation, Rangal and Baralaba coal measures with the overlying Rewan Group, Within a palynological framework, defining the P–T boundary in Australia has been particularly challenging due to several factors, including the apparently multiple floral turnovers during the transition from the late Permian Glossopterid flora to the Early Triassic flora, widespread erosional surfaces related to the rapidly aridifying climate, and a disconnect between the extinction event, negative carbon isotopic excursion (Retallack and Krull, 2006), and the GSSP-defined boundary. The boundary was initially thought to lie at or near the base of the *Kraeuselisporites saeptatus* and *Lunatisporites pellucidus* zones of western and eastern Australia, respectively (Dolby and Balme, 1976), correlative with the base of the informal eastern Australian unit APT1 of Price et al. (1985; see Price, 1997). Recent high-resolution radiometric analyses, however, indicate that the boundary may be situated stratigraphically lower (Laurie et al., 2016), i.e., at or near the base of the *Protohaploxypinus microcorpus* zone (including the *Playfordiaspora crenulata* (sub)zone; see Helby et al., 1987) equivalent to unit APP6 of Price et al. (1985; see Price, 1997). The Marker Mudstone was selected for further scrutiny of the palynostratigraphic data and age assignments as it appears to represent continuous deposition at the interface of the Bandanna and Rewan formations, and is fine-grained and organic-rich, which is ideal for palynological sampling and organic carbon isotope analysis.

## 3. Materials and methods

### 3.1. Study area

The borehole GSQ Tambo 1-1A is located on the Springsure Shelf in the south-east of the Galilee Basin (Fig. 1) and features a lithostratigraphic succession easily correlative with that of the Bowen Basin and a 1 m thick expression of the Marker Mudstone with no discernible unconformity at the base of the Rewan Formation.

### 3.2. Palynological processing and analysis

Twenty-two (22) samples were taken throughout the 45 m thick sequence for palynological and palynofacies analysis. Intervals sampled included the siltstones

above the Marker Mudstone (TAMP1–TAMP6), the Marker Mudstone itself (TAMP7–TAMP11) and siltstones and mudstones in the underlying Bandanna Formation and 'Burngrove Formation' equivalent (TAMP12–TAMP22). A 20 m thick sandstone interval separates samples TAMP1–TAMP12 and TAMP13–TAMP22.

Acid-processing of palynological samples was conducted by MGPalaeo laboratory in Perth. Standard acid processing techniques were used (Wood et al., 1996). This involved digesting 15–20 g of sample in HCl to remove carbonates. Excess HCl was decanted and HF was added to remove silicates. After 48 hours the excess acid was decanted and neutralised by repeated washings in deionised $H_2O$ and centrifuging. The residue then underwent density separation using heavy liquid (density 2.0) and was mounted on a slide. Two slides per sample were prepared using this method, and two more were prepared after oxidation with $HNO_3$ to remove palynodebris.

Analysis and counting of palynological slides was done using a Zeiss Photomicroscope III equipped with a Leica MC190HD camera. For biostratigraphy, counts of 200 palynomorphs per slide were done as per the recommendation of Traverse (2007). Classification of species was based on the nomenclature of Price (1997), Foster (1979, 1982), Backhouse (1991), de Jersey (1979) and Rigby and Hekel (1977). If taxonomic names differ between the authors, the most recently published names are used. Biostratigraphic assessment was based on the scheme of Price et al. (1985) and Price (1997). For palynofacies, counts of a minimum of 300 particles per sample were done. Particles were classified according to a palynofacies scheme based on that of Tyson (1995). Biostratigraphic and palynofacies data were plotted using the TILIA software package and statistically analysed using the CONISS cluster analysis to differentiate biozones and palynofacies assemblages. Count results were also plotted using ternary diagrams based on major palynofacies components (opaque phytoclasts, translucent phytoclasts, and terrestrial palynomorphs) to distinguish between different palynofacies assemblages.

### 3.3. Carbon isotope processing and analysis

Seventeen (17) samples of the total twenty-two (22) were crushed to powder for organic carbon isotope analysis at the University of Queensland, Australia. Isotope samples were compared to palynological samples taken at the equivalent depths to identify any co-occurring trends. The $\delta^{13}C$ isotope values were determined with a

stable-isotope-ratio mass spectrometer (Isoprime), coupled in continuous flow mode with an elemental analyser (Elementar Cube) (EA-CF-IRMS). Calibration was performed by use of two standards, USGS24 (-16.1‰ $\delta^{13}$CPDB) and NAT76H (-29.26‰ $\delta^{13}$CPDB), which were interspersed throughout analytical runs. Each sample was analysed in duplicate, using 50–200 μg of concentrate combusted at 1020°C in 3.5 mm × 5 mm tin capsules. Any sample with a beam size outside the working range of 1 × 10–9 to 9 × 10–9 Å, or with a $\delta^{13}$C result variation between duplicates of > 0.4‰, was re-analysed, in accordance with laboratory quality control practices.

## 4. Results

### 4.1. Palynostratigraphy

Of the twenty-two samples processed for palynology, thirteen yielded assemblages suitable for palynomorph counting (Fig. 4). These samples were TAMP1, TAMP3, TAMP4, TAMP9, TAMP10, TAMP11, TAMP16, TAMP17, TAMP18, TAMP19, TAMP20, TAMP21 and TAMP22. Samples TAMP5–TAMP8 yielded a few poorly preserved palynomorphs, though these were generally covered in degraded phytoclasts (Fig. 8A) and counts were not possible; the few species that were identifiable in these samples were noted.

Samples TAMP16–TAMP22 all yielded assemblages typical of unit APP5 (Price et al., 1985) characterized by a high abundance and diversity of striate bisaccate pollen grains (*Protohaploxypinus* spp., *Striatopodocarpites* spp.) and non-striate bisaccate pollen grains (*Alisporites* spp., *Scheuringipollenites* spp., *Vitreisporites pallidus*). Spinose and ornamented trilete spores (*Microbaculispora* spp., *Horriditriletes* spp.) are also common, as are monosulcate pollen grains (*Marsupipollenites* spp.). *Dulhuntyispora parvithola*, the index taxon of unit APP5, was not identified within these samples, but *Microreticulatisporites bitriangularis* (Fig. 8E), the key taxon of the APP5005 subunit, is a rare component in many of the samples. *Lycopodiumsporites* '*crassus*', the index taxon for the APP5006 subunit was neither detected in this study; hence, the samples were placed within the APP5005 subunit. The Marker Mudstone samples (samples TAMP9–TAMP11) yielded assemblages closely resembling those of the samples stratigraphically lower in the section, with some notable differences. The abundances of the smooth-walled trilete spore *Leiotriletes directus* and the ornamented trilete spore *Brevitriletes* spp. increase,

whereas the abundance of the previously dominant pollen species *Protohaploxypinus limpidus* decreases.

Samples TAMP1, TAMP3 and TAMP4 feature an assemblage distinctly different to those of the Marker Mudstone. Samples TAMP3 and TAMP4 both contain rare specimens of *Playfordiaspora crenulata* (Fig. 8B), the index taxon for the lower *P. microcorpus* biozone of Foster (1979). Sample TAMP1 further contains several specimens of *Triquitrites proratus* and *Tigrisporites playfordii*, both of which are also indicative of unit APP6. Other significant species featured in samples TAMP3 and TAMP4 include small ornamented trilete spores (*Thymospora ipsviciensis*, *Brevitriletes* spp.) and spinose trilete spores (*Horriditriletes* spp.). The abundance and diversity of bisaccate pollen grains has decreased. Smooth-walled trilete spores (*Leiotriletes directus*, *Calamospora* sp., *Punctatisporites* spp.) are particularly abundant in sample TAMP1.

**4.2. Palynofacies**

The samples taken from below the Marker Mudstone (TAMP12–TAMP22) feature varied palynofacies assemblages, but distinct trends can be recognized (Fig. 5). The proportion of opaque phytoclasts tends to increase up-section, though there is some variance (between 69.2% and 31.3% of the total assemblage). Equidimensional phytoclasts are the most abundant component of the assemblage, but structured and unstructured translucent phytoclasts are also common. Sporomorphs (particularly bisaccate pollen grains) have high relative abundance in TAMP21, TAMP20 and TAMP19, with palynomorphs outnumbering even the phytoclasts. The palynomorph abundance decreases up-section as the sandstone intervals become thicker until the assemblage features little to no palynomorphs preserved. Acanthomorph acritarchs and fungal spores are absent from this interval, but *Botryococcus* and *Cymatiosphaera* are present in rare abundances (Fig. 9). TAMP12, located slightly below the Marker Mudstone, features an assemblage dominated by opaque phytoclasts, with very few palynomorphs preserved but the highest proportion of amorphous organic matter (AOM) found in any of the studied samples.

The samples taken from the Marker Mudstone (TAMP7–TAMP11) show a striking trend with regard to oxidation of the phytoclasts. Sample TAMP11 features an assemblage dominated by translucent phytoclasts. The abundance of translucent phytoclasts decreases up-section whereas the opaque phytoclasts become dominant.

AOM is present in low abundance in all samples within the Marker Mudstone, and degraded phytoclasts have a spike in sample TAMP8. The degraded phytoclasts are an unusual component of the assemblage as they appear to occur in the form of clusters of fragments of opaque and translucent phytoclast debris surrounded by a pseudoamorphous groundmass. Pollen and spores are rare, and indeterminate palynomorphs tend to be more abundant in TAMP7 and TAMP8. The Marker Mudstone contains rare *Botryococcus*, as well as acanthomorph acritarchs (*Micrhystridium*) and fungal remains (*Reduviasporonites chalastus*). Above the Marker Mudstone, samples TAMP1, TAMP2, TAMP5 and TAMP6 all have very high abundances of opaque phytoclasts and low abundances of translucent phytoclasts and palynomorphs. Samples TAMP5 and TAMP6 also feature low abundances of degraded phytoclasts. Samples TAMP3 and TAMP4 represent a distinct shift to an assemblage with even abundances of opaque and translucent phytoclasts and with higher abundances of palynomorphs. *Botryococcus*, acanthomorph acritarchs, and fungal remains are all present in low abundances in these samples as well (Fig. 9).

Results of our cluster analysis reveal three distinct palynofacies assemblages (Fig. 10). Samples TAMP19–TAMP21 encompass Assemblage A, which is mainly characterised by the high abundance of terrestrial palynomorphs (> 30%) relative to the proportion of phytoclasts. Samples TAMP3, TAMP4, TAMP9, TAMP10, TAMP11, TAMP13, TAMP15, TAMP16 and TAMP17 are classified as part of Assemblage B, which is characterised by a lower proportion of opaque phytoclasts (< 60%) relative to the translucent phytoclasts and lower proportions of terrestrial palynomorphs (< 30%). Assemblage C (samples TAMP1, TAMP2, TAMP5, TAMP6, TAMP7, TAMP8, TAMP12, TAMP14, TAMP18, and TAMP22) is characterised by very high proportions of opaque phytoclasts (> 60%) and relatively low proportions of terrestrial palynomorphs (< 30%).

### 4.3. Carbon isotopes

The values of organic $\delta^{13}C$ within the Tambo 1-1A samples range from -26.2‰ to -23.2‰ (Table 1), typical for Permian-age coals (Korte and Kozur, 2010). At core depths shallower than 723.73 m, the $\delta^{13}C$ values deplete significantly to an absolute minimum of -26.2‰ at 700.39 m. From the data it is possible to distinguish two clear data ranges: the upper data range occurring in TAMI1–TAMI7 with an average $\delta^{13}C$ of -25.8‰ ($\sigma$ = 0.3‰), and the lower data range within TAMI8–TAMI17 with an

average $\delta^{13}C$ of -23.6‰ ($\sigma$ = 0.3‰). These two data ranges are separated by a maximum $\Delta$ 3.0‰ isotopic excursion. This relatively low magnitude excursion is comparable to other organic carbon isotopic values in Australia during the preliminary stages of $CO_2$ release, prior to the Permian–Triassic boundary (Retallack and Krull, 2006). Carbon isotopic values indicate no observable trends with palynofacies data, indicating that $\delta^{13}C$ is not dependent on phytoclast type or assemblage.

## 5. Discussion

### 5.1. Age determination – Unit APP6

The onset of unit APP6 or equivalent biostratigraphic units shows some degree of variability across the eastern Australian basins. Michaelsen (2002) mark its appearance at the base of the Marker Mudstone, while Rigby and Hekel (1977) and de Jersey (1979) mark the stratigraphic position of the Permian–Triassic boundary just above the uppermost coal seam. Difficulties arise due to the distinction of the *Playfordiaspora crenulata* and *Protohaploxypinus microcorpus* zones (Foster, 1979). This is due to the appearance of forms resembling *P. microcorpus* below the level of the first appearance of *P. crenulata* (this work; de Jersey, 1979; McLoughlin, 1988; Price, 1997). Foster (1979, 1982) proposed a subzone *P. microcorpus* Zone as defined by Helby (1973) using the first appearance of *P. crenulata* to define a lower unit. Initially this was described as the Lower *P. microcorpus* Zone, but later it was amended to become the *P. crenulata* Oppel zone based on its biostratigraphic and geographic significance (Foster, 1982). Unit APP6 was initially defined by Price (1997), based on the first appearance of *Triplexisporites playfordii*. However, the subunits of APP601 and APP602 were equated with the *P. crenulata* and *P. microcorpus* associations, respectively. Many of the elements present within APP5005 subunit continue to appear within the lower APP6 unit though in much lower abundances (*Protohaploxypinus, Scheuringipollenites*), along with the appearance of several new key species (e.g., *Triquitrites proratus, Triplexisporites playfordii*). However, the samples examined in this work as well as the datasets of de Jersey (1979) show that the appearance of key index taxa marking the onset of unit APP6 do not necessarily appear in the same horizon, which suggests strong environmental or sedimentological controls on the base and extent of the APP6 unit.

### 5.2. Permian–Triassic boundary

Placing the unit APP6 relative to the Permian–Triassic boundary in eastern Australia has challenged workers in the area for many decades. The presence of key P–T indicators such as macrofloral turnover and fungal spikes is inconsistent and so workers have turned to chronostratigraphic techniques. Metcalfe et al. (2015) used high precision U-Pb zircon dates to place the GSSP-defined P–T boundary in the Scarborough Sandstone uncoupling it from the extinction interval, which is located at the base of the Coalcliff Sandstone. This would place the extinction interval at the base of unit APP6 and the GSSP-defined P–T boundary into the lower part of unit APT1. Laurie et al. (2016) place the unit APP6 in the earliest Triassic on the basis of palynological and macrofloral data from the borehole Santos Yebna 1 (Powis, 2009). The base of the unit APP6 was defined at this locality just above the uppermost Permian coal seam by the first appearance of *Triplexisporites playfordii* (Murdoch, 2012). Several metres above this interval, Powis (2009) recorded non-glossopterid macroflora, which may suggest a post-extinction plant assemblage. U-Pb zircon dates were also used to calibrate the biostratigraphic scheme, placing the P–T boundary at the base of unit APP6, however no ages have so far been obtained from unit APP6 itself to support this interpretation (Laurie et al., 2016). In the Sydney Basin, Retallack (1995) associates the *P. microcorpus* Zone with the *Dicroidium callipteroides* megafloral biozone in the Early Triassic and identifies a distinct change from a high diversity glossopterid flora to a low diversity post-extinction flora just above the Bulli Coal.

In Antarctica, the P–T boundary sections are well exposed. Collinson et al. (2006) identify the *P. microcorpus* Zone from a sample at the base of a carbonaceous mudstone parting in the uppermost Permian coals in the Buckley Formation at Graphite Peak. *Vertebraria* (glossopterid roots) were recovered several centimetres above the top of the mudstone parting at the base of the uppermost coal seam in the Buckley Formation (Retallack and Krull, 1999), which suggests the extinction interval lies above their sampled interval. The *P. microcorpus* flora is regarded as transitional between the *Glossopteris* vegetation and the final extinction event, which eliminates the last elements of the *Glossopteris* flora. In a section studied in the Prince Charles Mountains, the P–T boundary was placed at the interface of the McKinnon Member and Ritchie beds, based on the cessation of coal deposition. This interval also marks

the first appearance of *Lunatisporites pellucidus*, the index taxon of unit APT1 (Lindström and McLoughlin, 2007). In the central Transantarctic Mountains, *Glossopteris* remains have been found 37 m above detrital zircon samples indicating an Early Triassic age (Elliot et al., 2017), while in South Africa, *Glossopteris* remains were recovered from the *Lystrosaurus* Assemblage Zone, which is regarded as Triassic in age (Gastaldo et al., 2017). Both these occurrences raise questions about the accuracy of proxies such as a macrofloral turnover when defining the terrestrial expression of the P–T boundary. Even in the marine basins of western Australia, placing the P–T boundary with confidence is a challenge due to unconformities in different sections in each basin and a lack of ashfall tuffs that can be age dated. However, in all basins the carbon isotopes tend to correlate well with the microfossil biostratigraphy (Gorter et al., 2009). The carbon isotope excursion begins to shift more negative at the base of the *P. microcorpus* Zone and reaches its most negative values at the base of the *L. pellucidus* Zone (Morante, 1996; Gorter et al., 2009), which agrees with the aforementioned Antarctic studies.

Using organic carbon isotopes, the age-proximity of the Marker Mudstone's deposition to the P–T boundary may be speculated. From the relatively low magnitude excursion observed in these samples, it is assumed that the Marker Mudstone was not deposited during a time period to which the full extent of contemporaneous $CO_2$ production occurred (Korte and Kozur, 2010). This interpretation is supported by the lack of observable unit APP6 taxa in the Marker Mudstone samples, which suggest the P–T boundary itself, and the apogee of the P–T carbon isotopic excursion occurred well after the deposition of the Marker Mudstone. The use of carbon isotope trends as tool for relative age dating across relatively low-resolution sequences is problematic, given a number of palaeoenvironmental factors that may influence the uptake of carbon isotopes in the primordial plant material (Van de Wetering et al., 2013b). It is these palaeoenvironmental factors that are attributed to the low magnitude ($\sigma = 0.3‰$) variation in carbon isotopic values within the upper (TAMI1–TAMI7) and lower (TAMI8–TAMI17) range of isotopic values for the Marker Mudstone, though these are not causally related to palynofacies changes observed within the equivalent samples. Furthermore, the absolute range and timing of carbon isotopic variation is variable between sample location and stratigraphy, dependent on both depositional setting and geographical proximity to the Siberian

Traps and late Permian volcanic systems associated with massive $CO_2$ expulsion (Svensen et al., 2009).

### 5.3. Palaeoenvironment

The presence of a variety of freshwater to brackish algae (*Botryococcus*, *Brazilea*) and prasinophytes (*Cymatiosphaera*) in the Bandanna Formation fits well with the previous interpretation of a deltaic environment (Fig. 7) (Phillips et al., 2017). The mudstones and siltstones at around 740 m in core Tambo 1-1A are the distal equivalent of the B seam (Fig. 3). This interval falls into palynofacies Assemblage A, an assemblage dominated by palynomorphs, particularly bisaccate pollen grains, which are concentrated in distal areas due to the Neves Effect (Chaloner and Muir, 1968). The section coarsens upwards into a more sandstone-dominated facies as the delta prograded southwards. The palynofacies also appear consistent with this interpretation with a transition from Assemblage A to Assemblage B featuring an increased abundance of phytoclasts, suggesting increased proximity to the terrestrial source with a switch to a fluvial-dominated environment. The phytoclast assemblage is a mixture of opaque and translucent phytoclasts, which reflects varying lengths of transport either from vegetation occupying the delta and adjacent swamps or from fluvial systems carrying phytoclasts over a long distance.

The occurrence of the black organic-rich Marker Mudstone along with the presence of acritarchs, albeit in low abundances, suggests that this bed may represent a maximum flooding surface. This coincides with a spike in acritarch abundances in the Sydney Basin immediately above the uppermost Permian coals (Bulli Coal), which Retallack (1995) attributed to a short-term marine incursion. The low abundances of freshwater/brackish algae and AOM could reflect either poor preservation or conditions in the water column unsuitable for the proliferation of freshwater algal colonies. The palynofacies assemblage shifts from Assemblage B to Assemblage C, suggesting a change in the oxidation conditions in the water column or a change in the transport dynamics affecting input into the lake. A similar trend can be seen in the transition from palynofacies CPFII to CPFIII in late Permian coal deposits (Van de Wetering et al., 2013a), where an assemblage featuring mixed opaque and translucent phytoclasts and very low AOM abundances is replaced by an assemblage almost completely dominated by opaque phytoclasts. This is related to a base-level change from high to fluctuating, with redox conditions changing from stable to oxic.

A high base level with anoxic bottom waters would preserve wood fragments and organic material in the sediments to form the organic-rich mudstone. The source of the degraded phytoclasts remains uncertain. They might derive from eroded peat further inland, or might indicate extreme conditions (i.e., high acidity) within the water column, both of which are phenomena typically associated with end-Permian environmental perturbation (Sephton et al., 2005, 2015).

Detrital-zircon data from Phillips et al. (2018) indicate that the Anakie Inlier was submerged at the time the Marker Mudstone was deposited, and that the waterbody was a large-scale feature that spread across both basins (Fig. 7). Accommodation for this waterbody would have been created by subsidence related to foreland loading on the eastern margin of the Bowen Basin. Thin sandstone beds sourced from the east occur within coarsening-upwards sequences above the Marker Mudstone and its regional equivalents (Grech and Dyson, 1997). These sandstones make up the basal unit of the Sagittarius Sandstone and may represent a proximal deltaic facies, which progrades westwards (Grech, 2001; Sliwa et al., 2017). The full extent of the Marker Mudstone is still not well constrained and it is yet to be determined if it represents a single extensive lake or smaller separate bodies of water which infilled the topography during the transgression. This might explain the apparent diachroneity in the palynogical correlation between basins (Sliwa et al., 2017).

The palynofacies above the Marker Mudstone is generally opaque phytoclast dominated and has a very low abundance of palynomorphs (Assemblage C), which may reflect long-distance transport in fluvial channels associated with the regressive Rewan Formation. An alternative interpretation is that this assemblage could potentially also represent a P–T extinction interval as fungal remains (*Reduviasporinites chalastus*) are present above and below, though in rare abundances. However, the switch back to Assemblage B only a few centimetres above this interval in samples TAMP3 and TAMP4, which contain a diverse APP6 flora, raises questions about the extent and position of the extinction event and about the P–T boundary placement in eastern Australia.

## 6. Conclusions and outlook

Palynological and palynofacies data from GSQ Tambo 1-1A provide new insight into the late Permian palaeoenvironment in the Galilee Basin. The data generally agree with previous interpretations of a prograding deltaic system, which then

subsided and was flooded with a large waterbody (lake) that occupied the potentially combined centre of the Bowen and Galilee basins due to a submerged Anakie Inlier (Phillips et al., 2017, 2018). The change in algal components with rare occurrences of acanthomorph acritarchs suggests an increased salinity level, potentially related to a short-term marine transgression.

Based on palynological data alone, we cannot place the P–T boundary in GSQ Tambo 1-1A with any certainty. Whereas the transition from unit APP5 to unit APP6 correlates well with some coeval sections in the Bowen Basin (Smith and Mantle, 2013) and Sydney Basin (Retallack, 1995), it differs from that of the Marker Mudstone section at the Newlands Coal Mine (Michaelsen et al., 2000), where the transition to unit APP6 lies at the base of the Marker Mudstone package. This suggests some degree of diachroneity, with regard to either the base of unit APP6 or the onset of the Marker Mudstone deposition. Another potential interpretation is that the "Marker Mudstone" featured in the Galilee Basin is not a true correlative of the Marker Mudstone mapped in the Bowen Basin. Carbon isotopic evidence from the Marker Mudstone concurs with palynological results, indicating the onset of contemporaneous $CO_2$ release at the onset of the P–T carbon isotopic excursion, but not coincident with the apogee of this event.

More detailed studies of the Marker Mudstone in both the Bowen and Galilee basins are needed to fully understand its relationship to the P–T boundary. Mapping of the Marker Mudstone in the Galilee Basin is needed to understand its nature and spatial distribution, for comparison with the Bowen Basin. Future studies should also focus not just on palynological data, but on high-resolution carbon isotope and trace element trends to allow more detailed interpretations of the palaeoenvironmental and palaeoclimatic changes occurring in Australia at the end of the Permian.

**Acknowledgements**

The authors would like to thank the Vale UQ Coal Geoscience Program for funding this study, and The Palynological Society – AASP for providing additional funding. Many thanks also to MGPalaeo and Dr. Kim Baublys for assistance with sample preparation. We would also like to extend our thanks to the reviewers Benjamin Bomfleur and Cortland Eble whose comments greatly improved the manuscript.

**References**

Allen, J.P., Fielding, C.R., 2007. Sequence architecture within a low-accommodation setting: An example from the Permian of the Galilee and Bowen basins, Queensland, Australia. AAPG Bulletin 91 (11), 1503–1539.

Backhouse, J., 1991. Permian palynostratigraphy of the Collie Basin, western Australia. Review of Palaeobotany and Palynology 67 (3–4), 237–314.

Benton, M.J., Twitchett, R.J., 2003. How to kill (almost) all life: the end-Permian extinction event. Trends in Ecology & Evolution 18 (7), 358–365.

Bercovici, A., Vajda, V., 2016. Terrestrial Permian–Triassic boundary sections in South China. Global and Planetary Change, 143, 31–33.

Brakel, A.T., Totterdell, J.M., Wells, A.T., Nicoll, M.G., 2009. Sequence stratigraphy and fill history of the Bowen Basin, Queensland. Australian Journal of Earth Sciences 56 (3), 401–432.

Chaloner, W.G., Muir, M., 1968. Spores and floras. In: Murchinson, D.G. (Ed.), Coal and Coal-bearing Strata. Oliver and Boyd, Edinburgh, pp. 127–146.

Collinson, J.W., Hammer, W.R., Askin, R.A., Elliot, D.H., 2006. Permian–Triassic boundary in the central Transantarctic Mountains, Antarctica. Geological Society of America Bulletin 118 (5–6), 747–763.

de Jersey, N.J., 1979. Palynology of the Permian–Triassic transition in the western Bowen Basin. Geological Survey of Queensland Publications 374. Palaeontological Papers 46, 1–39.

de Wit, M.J., Ghosh, J.G., de Villiers, S., Rakotosolofo, N., Alexander, J., Tripathi, A., Looy, C., 2002. Multiple organic carbon isotope reversals across the Permo-Triassic boundary of terrestrial Gondwana sequences: clues to extinction patterns and delayed ecosystem recovery. The Journal of Geology 110 (2), 227–240.

Dolby, J.H., Balme, B.E., 1976. Triassic palynology of the Carnarvon Basin, western Australia. Review of Palaeobotany and Palynology 22 (2), 105–168.

Elliot, D.H., Fanning, C.M., Isbell, J.L., Hulett, S.R., 2017. The Permo-Triassic Gondwana sequence, central Transantarctic Mountains, Antarctica: zircon geochronology, provenance, and basin evolution. Geosphere 13 (1), 155–178.

Eshet, Y., Rampino, M.R., Visscher, H., 1995. Fungal event and palynological record of ecological crisis and recovery across the Permian–Triassic boundary. Geology 23 (11), 967–970.

Foster, C.B., 1979. Permian plant microfossils of the Blair Athol Coal Measures, Baralaba Coal Measures, and basal Rewan Formation of Queensland. Geological Survey of Queensland Publications 372. Palaeontological Papers 45, 1–244.

Foster, C.B., 1982. Spore-pollen assemblages of the Bowen Basin, Queensland (Australia): their relationship to the Permian/Triassic boundary. Review of Palaeobotany and Palynology 36 (1–2), 165–183.

Foster, C.B., Stephenson, M.H., Marshall, C., Logan, G.A., Greenwood, P.F., 2002. A revision of *Reduviasporonites* Wilson 1962: description, illustration, comparison and biological affinities. Palynology 26 (1), 35–58.

Gastaldo, R.A., Neveling, J., Clark, C.K., Newbury, S.S., 2009. The terrestrial Permian–Triassic boundary event bed is a nonevent. Geology 37 (3), 199–202.

Gastaldo, R.A., Neveling, J., Looy, C.V., Bamford, M.K., Kamo, S.L., Geissman, J.W., 2017. Paleontology of the Blaauwater 67 and 65 Farms, South Africa: testing the *Daptocephalus*/*Lystrosaurus* biozone boundary in a stratigraphic framework. Palaios 32 (6), 349–366.

Gorter, J., Nicoll, R.S., Metcalfe, I., Willink, R., Ferdinando, D., 2009. The Permian–Triassic boundary in Western Australia: evidence from the Bonaparte and Northern Perth basins — exploration implications. The APPEA Journal 49 (1), 311–336.

Grech, P.V.J.W., 2001. Sedimentology and sequence stratigraphy of the Early Triassic Rewan Group, Bowen Basin. PhD Thesis, University of Adelaide, 394 pp.

Grech, P.V., Dyson, I.A., 1997. An integrated approach to the study of the Early Triassic Rewan Group, Bowen Basin. The APPEA Journal 37 (1), 192–204.

Hansen, J., Uroda, A., 2018. Reinterpretation of wire-line log data in the eastern Galilee Basin, Queensland: Stratigraphical and hydrogeological implications. ASEG Extended Abstracts 2018 (1), 1–8.

Helby, R., 1973. Review of Late Permian and Triassic palynology of New South Wales. Geological Society of Australia Special Publication 4, 141–155.

Helby, R., Morgan, R., Partridge, A.D., 1987. A palynological zonation of the Australian Mesozoic. Memoirs of the Association of Australasian Palaeontologists 4, 1–94.

Hobday, D.K., 1987. Gondwana coal basins of Australia and South Africa: tectonic setting, depositional systems and resources. Geological Society, London, Special Publications 32 (1), 219–233.

Hochuli, P.A., 2016. Interpretation of "fungal spikes" in Permian–Triassic Boundary sections. Global and Planetary Change 144, 48–50.

I'Anson, A., Deighton, I., Müller, R.D., Dutkiewicz, A., Heine, C., 2018. Burial and exhumation history of the Galilee Basin, Australia: Implications for unconventional hydrocarbon prospectivity. AAPG Bulletin 102 (3), 483–507.

Korte, C., Kozur, H.W., 2010. Carbon-isotope stratigraphy across the Permian–Triassic boundary: A review. Journal of Asian Earth Sciences 39 (4), 215–235.

Laurie, J.R., Bodorkos, S., Nicoll, R.S., Crowley, J.L., Mantle, D.J., Mory, A.J., Champion, D.C., 2016. Calibrating the middle and late Permian palynostratigraphy of Australia to the geologic time-scale via U-Pb zircon CA-IDTIMS dating. Australian Journal of Earth Sciences 63 (6), 701–730.

Lindström, S., McLoughlin, S., 2007. Synchronous palynofloristic extinction and recovery after the end-Permian event in the Prince Charles Mountains, Antarctica: implications for palynofloristic turnover across Gondwana. Review of Palaeobotany and Palynology 145 (1–2), 89–122.

McLoughlin, S., 1988. Geology of the Inglis Dome, Denison Trough, central Queensland. Papers of the Department of Geology, University of Queensland 12, 229–263.

Metcalfe, I., Crowley, J.L., Nicoll, R.S., Schmitz, M., 2015. High-precision U-Pb CA-TIMS calibration of middle Permian to lower Triassic sequences, mass extinction and extreme climate-change in eastern Australian Gondwana. Gondwana Research 28 (1), 61–81.

Michaelsen, P., 2002. Mass extinction of peat-forming plants and the effect on fluvial styles across the Permian–Triassic boundary, northern Bowen Basin, Australia. Palaeogeography, Palaeoclimatology, Palaeoecology 179 (3–4), 173–188.

Michaelsen, P., Henderson, R.A., Crosdale, P.J., Mikkelsen, S.O., 2000. Facies architecture and depositional dynamics of the Upper Permian Rangal coal measures, Bowen Basin, Australia. Journal of Sedimentary Research 70 (4), 879–895.

Morante, R., 1996. Permian and early Triassic isotopic records of carbon and strontium in Australia and a scenario of events about the Permian–Triassic boundary. Historical Biology 11 (1–4), 289–310.

Murdoch, C., 2012. Palynostratigraphic analysis, Yebna 1, PL 232, Bowen Basin. Santos Stratigraphic Services, Palynology Report 2010/34 (unpublished report).

Phillips, L.J., Esterle, J.S., Edwards, S.A., 2017. Review of Lopingian (upper Permian) stratigraphy of the Galilee Basin, Queensland, Australia. Australian Journal of Earth Sciences 64 (3), 283–300.

Phillips, L.J., Crowley, J.L., Mantle, D.J., Esterle, J.S., Nicoll, R.S., McKellar, J.L., Wheeler, A., 2018. U-Pb geochronology and palynology from Lopingian (upper Permian) coal measure strata of the Galilee Basin, Queensland, Australia. Australian Journal of Earth Sciences 65 (2), 153–173.

Powis, G., 2009. Sequence stratigraphy of the Yebna 1 core, 1110–1320 m. Geodelta Pty Ltd., Noosa Heads, Queensland (unpublished report).

Price, P.L., 1997. Permian to Jurassic palynostratigraphic nomenclature of the Bowen and Surat Basins. In: Green, P.M. (Ed.), The Surat and Bowen Basins, Southeast Queensland. Queensland Department of Mines and Energy, Brisbane, pp. 137–178.

Price, P.L., Filatoff, J., Williams, A.J., Pickering, S.A., Wood, G.R., 1985. Late Palaeozoic and Mesozoic palynostratigraphical units. CSR Oil and Gas Division, Palynology Laboratory Report No. 274/25.

Retallack, G.J., 1995. Permian–Triassic life crisis on land. Science 267 (5194), 77–80.

Retallack, G.J., Krull, E.S., 1999. Landscape ecological shift at the Permian–Triassic boundary in Antarctica. Australian Journal of Earth Sciences 46 (5), 785–812.

Retallack, G.J., Krull, E.S., 2006. Carbon isotopic evidence for terminal-Permian methane outbursts and their role in extinctions of animals, plants, coral reefs, and peat swamps. GSA Special Papers 399, 249–269.

Rigby, J.F., Hekel, H., 1977. Palynology of the Permian sequence in the Springsure Anticline, central Queensland. Geological Survey of Queensland Publications 363. Palaeontological Papers 37, 1–76.

Sephton, M.A., Looy, C.V., Brinkhuis, H., Wignall, P.B., De Leeuw, J.W., Visscher, H., 2005. Catastrophic soil erosion during the end-Permian biotic crisis. Geology 33 (12), 941–944.

Sephton, M.A., Jiao, D., Engel, M.H., Looy, C.V., Visscher, H., 2015. Terrestrial acidification during the end-Permian biosphere crisis? Geology 43 (2), 159–162.

Sliwa, R., Esterle, J., Phillips, L., Wilson, S., 2017. Rangal Supermodel 2015: The Rangal-Baralaba-Bandanna Coal Measures in the Bowen and Galilee Basins. ACARP (Australian Coal Industry Research Program), Final Report ACARP Project C22028.

Smith, R.M., Botha-Brink, J., 2014. Anatomy of a mass extinction: sedimentological and taphonomic evidence for drought-induced die-offs at the Permo-Triassic boundary in the main Karoo Basin, South Africa. Palaeogeography, Palaeoclimatology, Palaeoecology 396, 99–118.

Smith, T.E., Mantle, D.J., 2013. Late Permian palynozones and associated CA-IDTIMS dated tuffs from the Bowen Basin, Australia. Geoscience Australia Record, Canberra, 2013/46, 45 pp.

Spina, A., Cirilli, S., Utting, J., Jansonius, J., 2015. Palynology of the Permian and Triassic of the Tesero and Bulla sections (Western Dolomites, Italy) and consideration about the enigmatic species *Reduviasporonites chalastus*. Review of Palaeobotany and Palynology 218, 3–14.

Steiner, M.B., Eshet, Y., Rampino, M.R., Schwindt, D.M., 2003. Fungal abundance spike and the Permian–Triassic boundary in the Karoo Supergroup (South Africa). Palaeogeography, Palaeoclimatology, Palaeoecology 194 (4), 405–414.

Svensen, H., Planke, S., Polozov, A.G., Schmidbauer, N., Corfu, F., Podladchikov, Y.Y., Jamtveit, B., 2009. Siberian gas venting and the end-Permian environmental crisis. Earth and Planetary Science Letters 277 (3–4), 490–500.

Traverse, A., 2007. Paleopalynology. 2nd ed. Springer, Berlin, 813 pp.

Tyson, R.V., 1995. Sedimentary Organic Matter: Organic Facies and Palynofacies. Chapman & Hall, London, 615 pp.

Van de Wetering, N., Esterle, J., Baublys, K., 2013a. Decoupling $\delta^{13}C$ response to palaeoflora cycles and climatic variation in coal: A case study from the Late Permian Bowen Basin, Queensland, Australia. Palaeogeography, Palaeoclimatology, Palaeoecology 386, 165–179.

Van de Wetering, N., Mendonça Filho, J.G., Esterle, J., 2013b. Palynofacies changes and their reflection on preservation of peat accumulation stages in the Late Permian coal measures of the Bowen Basin, Australia: A new system for coal palynofacies characterisation. International Journal of Coal Geology 120, 57–70.

Van Heeswijck, A., 2010. Late Paleozoic to early Mesozoic deformation in the northeastern Galilee Basin, Australia. Australian Journal of Earth Sciences 57 (4), 431–451.

Visscher, H., Brinkhuis, H., Dilcher, D.L., Elsik, W.C., Eshet, Y., Looy, C.V., Traverse, A., 1996. The terminal Paleozoic fungal event: evidence of terrestrial ecosystem destabilization and collapse. Proceedings of the National Academy of Sciences 93 (5), 2155–2158.

Wood, G.D., Gabriel, A.M., Lawson, J.C., 1996. Palynological techniques — processing and microscopy. In: Jansonius, J., McGregor, D.C. (Eds.), Palynology: Principles and Applications. American Association of Stratigraphic Palynologists Foundation 1, 29–50.

Yin, H.F., Zhang, K.X., Tong, J.N., Yang, Z.Y., Wu, S.B., 2001. The global stratotype section and point (GSSP) of the Permian–Triassic boundary. Episodes 24 (2), 102–114.

**Figure and table captions**

Figure 1. Map of the Galilee and Bowen basins with location of stratigraphically significant wells. GSQ Tambo 1-1A (marked with a star) occupies a position at the edge of the Springsure Shelf, which connects the two basins.

Figure 2. W-E cross section of the Permo-Triassic sediments infilling the Cooper, Galilee and Bowen basins overlain by the younger sediments of the Eromanga Basin (after Hobday, 1987).

Figure 3. Lithostratigraphic scheme of the Galilee Basin and Denison Trough (modified from Phillips et al., 2017). The relative positions of the major coal seams (A-F) are also displayed. Though there is evidence of a regional unconformity in many locations, the interface of the Bandanna and Rewan formations features the Marker Mudstone, and no unconformity is apparent. The interval being investigated in this study is marked between the two stars.

Figure 4. Palynostratigraphic data showing selected species from Tambo 1-1A based on counts of 200 palynomophs. Samples in which this count could not be reached are not included. The data indicates unit APP5 (?APP5006 subunit) continues into the Marker Mudstone. The transition to unit APP6 occurs above the mudstone (marked by the first sparse occurrence of *Protohaploxypinus microcorpus*). Cluster analysis suggests the assemblages in each unit are relatively distinct from one another even though some elements of unit APP5 are still present above the Marker Mudstone.

Figure 5. Line chart depicting palynofacies data from Tambo 1-1A. Lines measuring relative abundance (%) also mark sample locations on the lithology. Presence of key palaeoenvironmental indicators (algae/prasinophytes, acritarchs, fungal spores) are also marked. Cluster analysis of the samples suggests three main palynofacies patterns. Ternary diagrams plotting the data based on the major palynofacies components show three distinct palynofacies assemblages (A-C). The major palynofacies components are opaque phytoclasts (OP), translucent phytoclasts (TP) and terrestrial palynomorphs (PAL).

Figure 6. Carbon isotope trends with depth in Tambo 1-1A showing a low magnitude excursion within the Marker Mudstone, plotted alongside the pollen/spore ratio, bioevents, biostratigraphy and palynofacies cluster analysis. The current placement of the P–T boundary in Australia (Laurie et al., 2016) is marked, though evidence from this study is not sufficient to define it conclusively in this locality.

Figure 7. Reconstruction of the potential palaeoenvironmental conditions of the Bandanna Formation (A) and the Marker Mudstone (B). Data from Tambo 1-1A supports the interpretation of a southwards-prograding delta which subsides as base level rises leading to the formation of a large waterbody (lake) across the Bowen and Galilee basins (Phillips et al., 2017, 2018). Blue arrows suggest areas where a potential marine transgression could have come in. The presence of both acanthomorph acritarchs and *Botryococcus* suggests increased salinity but not fully open marine conditions, leading to the interpretation of a marine influenced lacustrine environment.

Figure 8. Phytoclasts, palynomorphs and fungal hyphae, borehole Tambo 1-1A (Galilee Basin). Taxon name is followed by sample number, slide number (brackets) and stage coordinates for a ZEISS Photomicroscope III. (A) Degraded phytoclasts, TAMP8 (b), 97.1/8.2. (B) *Playfordiaspora crenulata*, TAMP4 (a), 91.8/0.2. (C) *Protohaploxypinus microcorpus*, TAMP6 (a), 114.3/17.8. (D) Fungal hyphae?, TAMP10 (b), 97.2/2.4. (E) *Microreticulatisporites bitriangularis*, TAMP18 (a), 100.3/12.2.

Figure 9. Palynomorphs of borehole Tambo 1-1A (Galilee Basin). Taxon name is followed by sample number, slide number (brackets) and stage coordinates for a ZEISS Photomicroscope III. (A) *Micrhystridium* sp., TAMP10 (b), 99.7/1.2. (B) *Cymatiosphaera gondwanensis*, TAMP17 (a), 87.2/3.3. (C) *Botryococcus* sp., TAMP22 (a), 80.8/13.9. (D) *Botryococcus*?, TAMP3 (a), 104.2/16.7. (E) *Reduviasporonites chalastus*, TAMP3 (a), 109.3/17.2.

Figure 10. Palynofacies of borehole Tambo 1-1A (Galilee Basin). (A) Palynofacies Assemblage A featuring a high proportion of palynomorphs, particularly bisaccate pollen. (B) Palynofacies Assemblage B featuring a moderate to high proportion of translucent phytoclasts (structured and unstructured) as well as a moderate proportion of opaque phytoclasts and some well-preserved palynomorphs. (C) Palynofacies Assemblage C featuring a high proportion of opaque phytoclasts and a low proportion of translucent phytoclasts; palynomorphs are rarely well preserved.

**Figures**

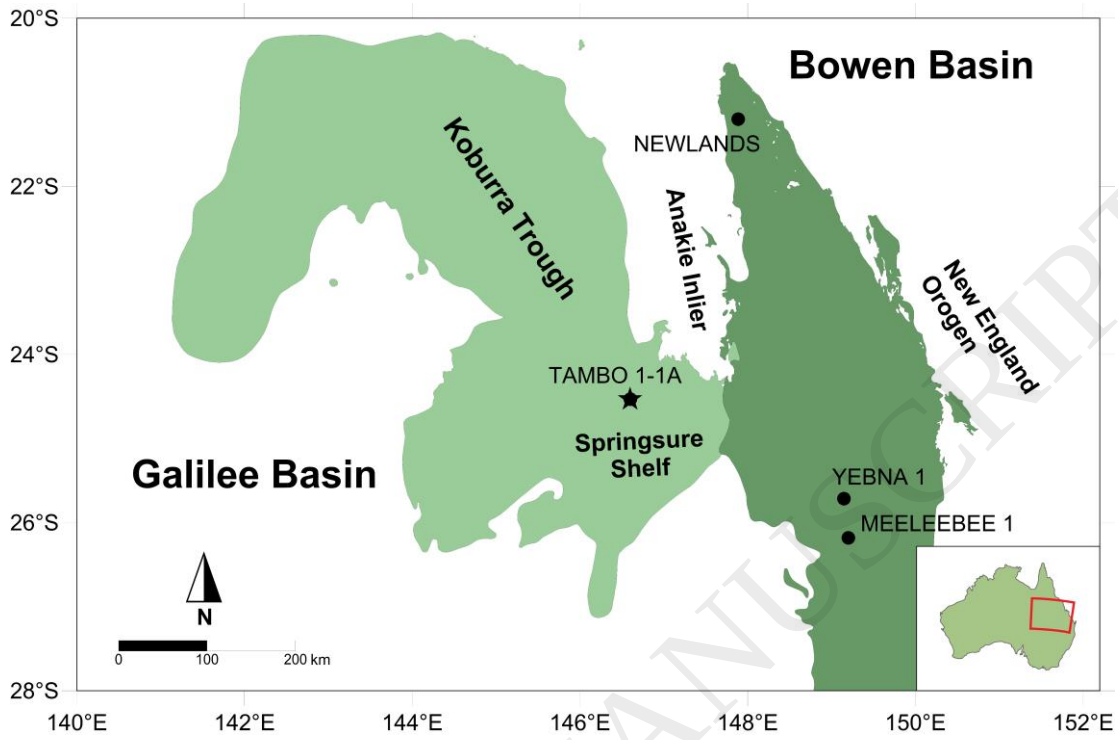


**Permian-Triassic basins**
A: Arckaringa
B: Bowen
C: Cooper
DT: Denison Trough
G: Gunnedah
GA: Galilee
O: Oaklands
P: Pedrika
R: Renmark Trough
S: Sydney
T: Tasmania

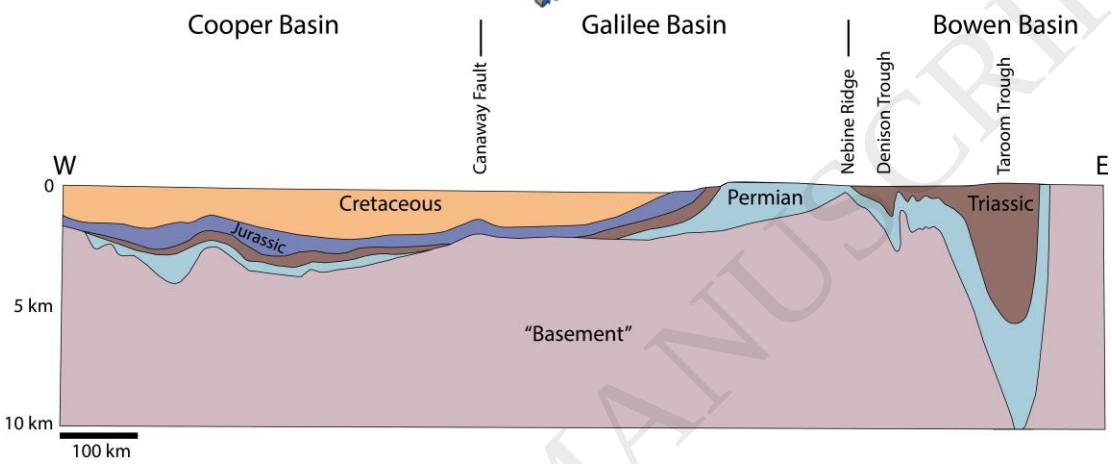


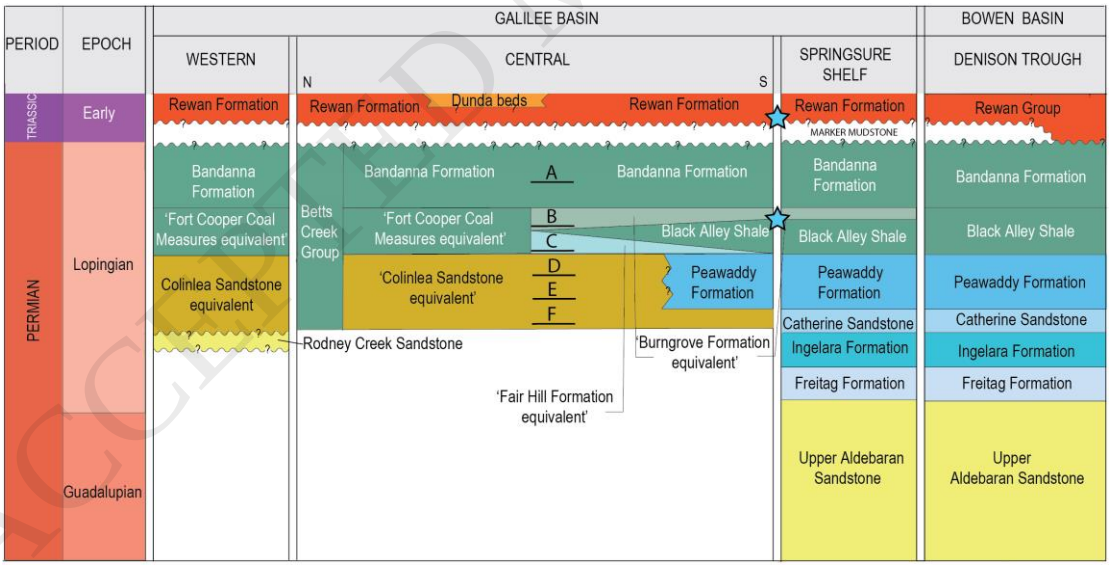

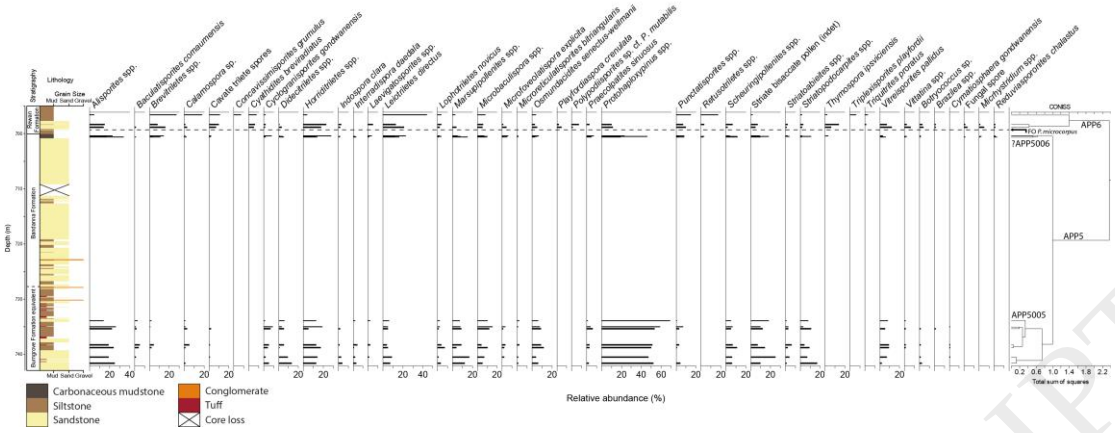


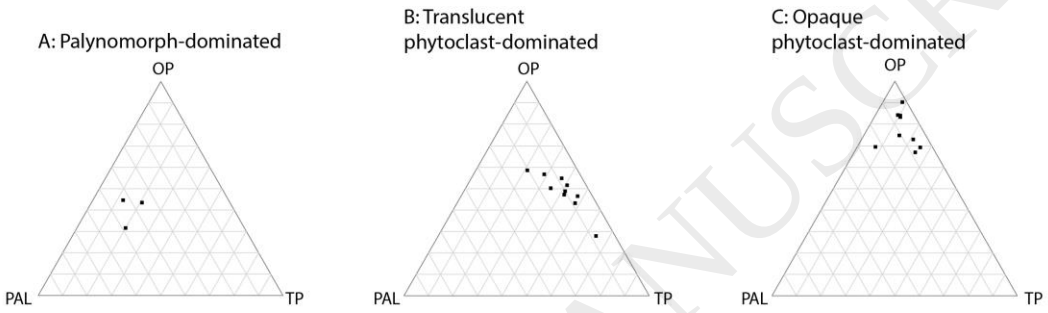


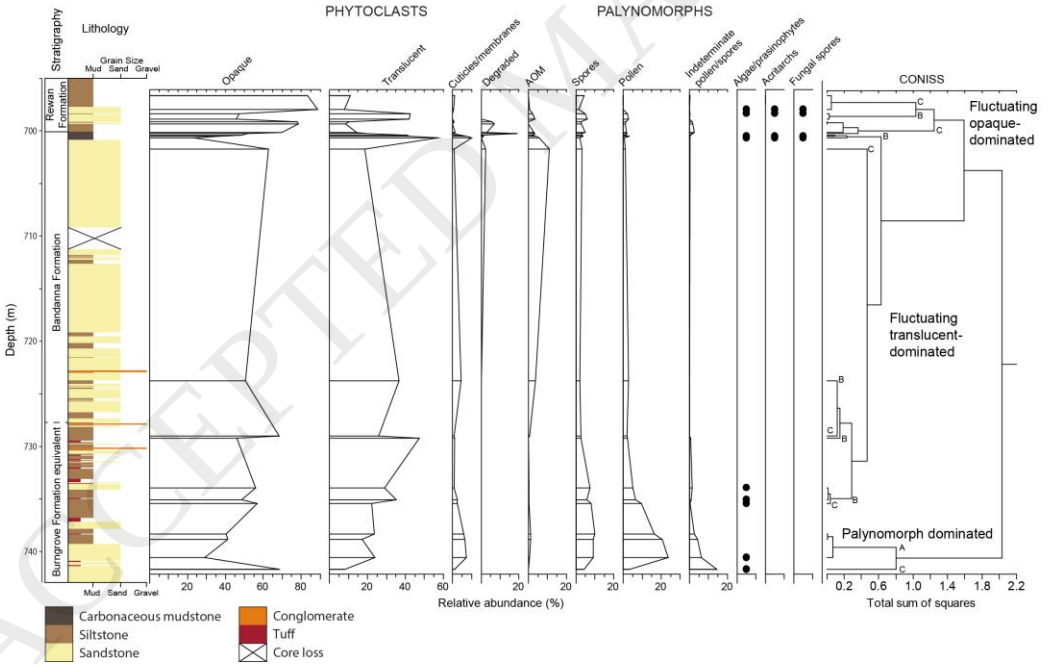

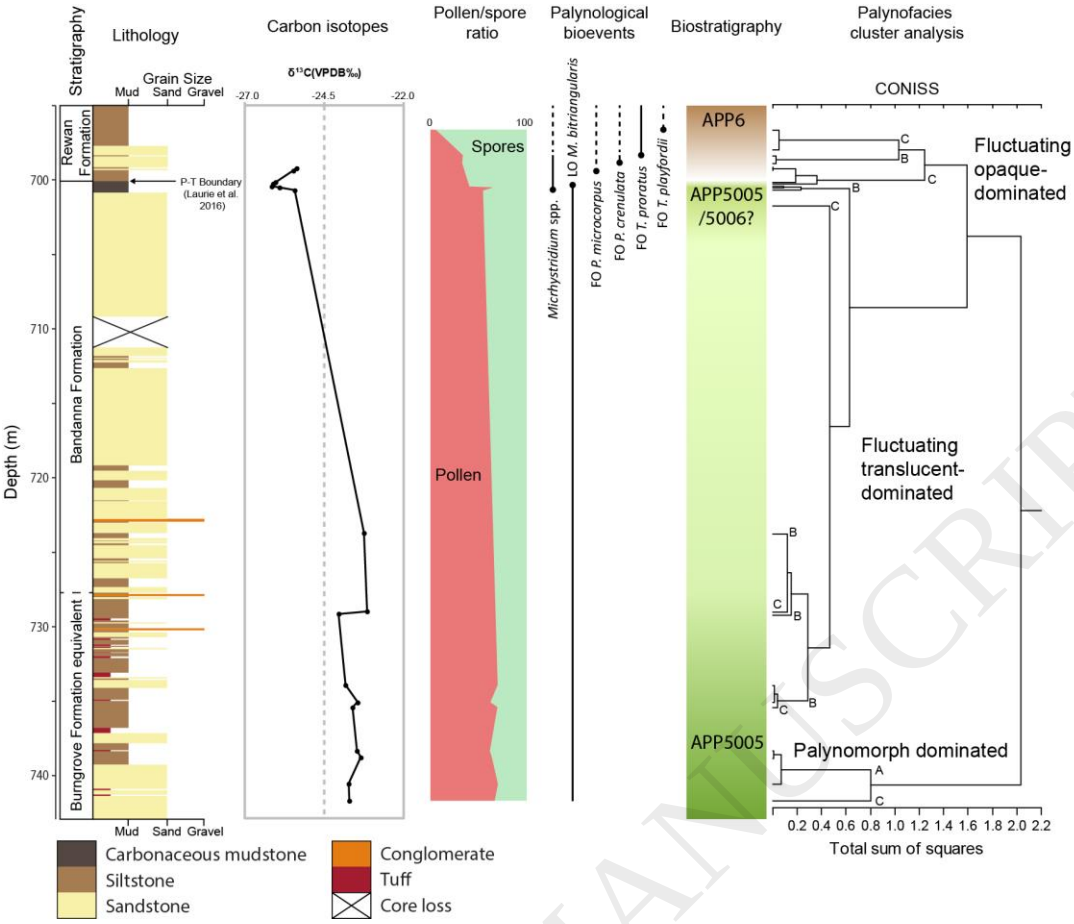


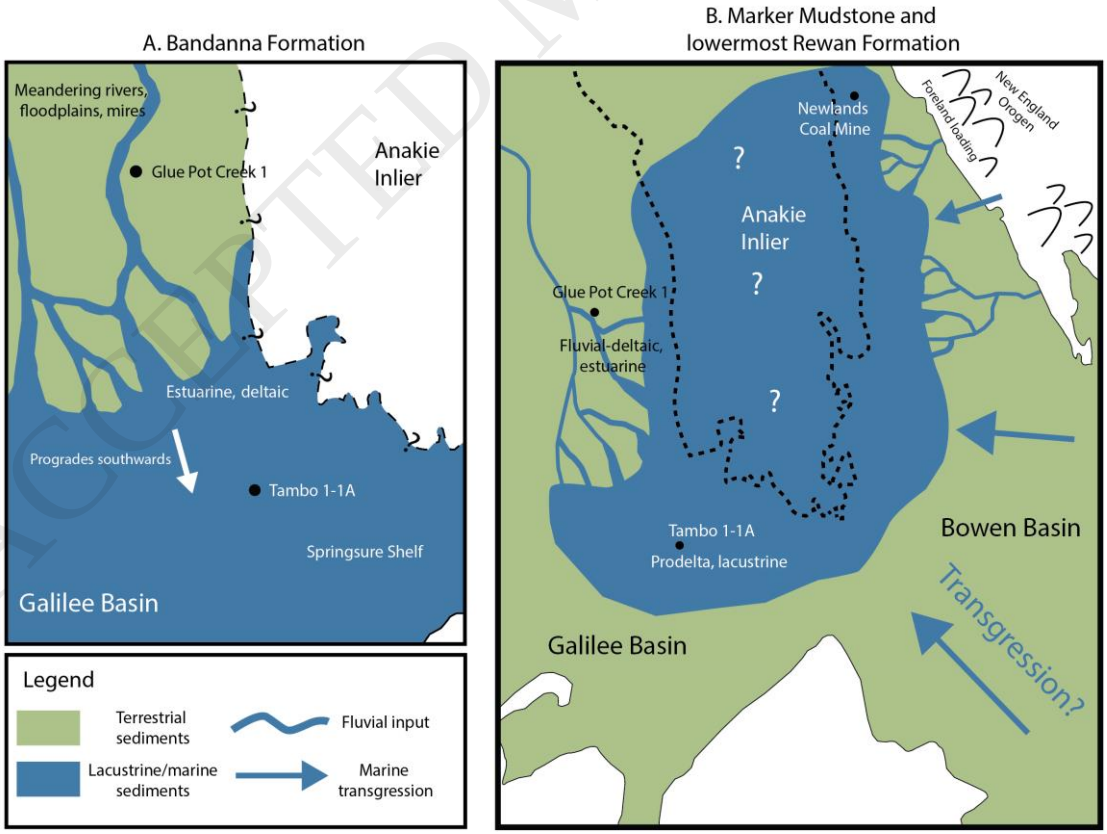

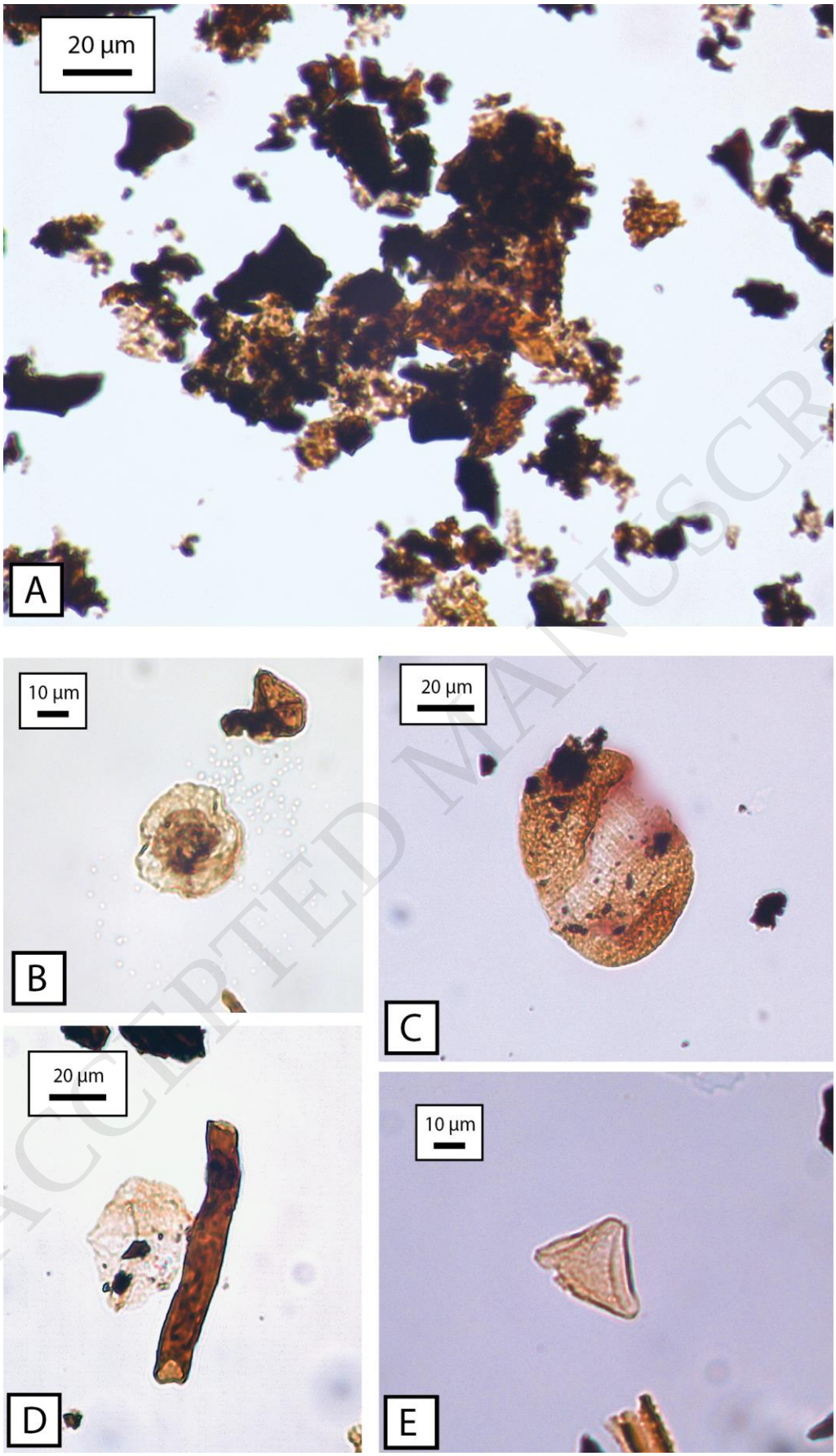

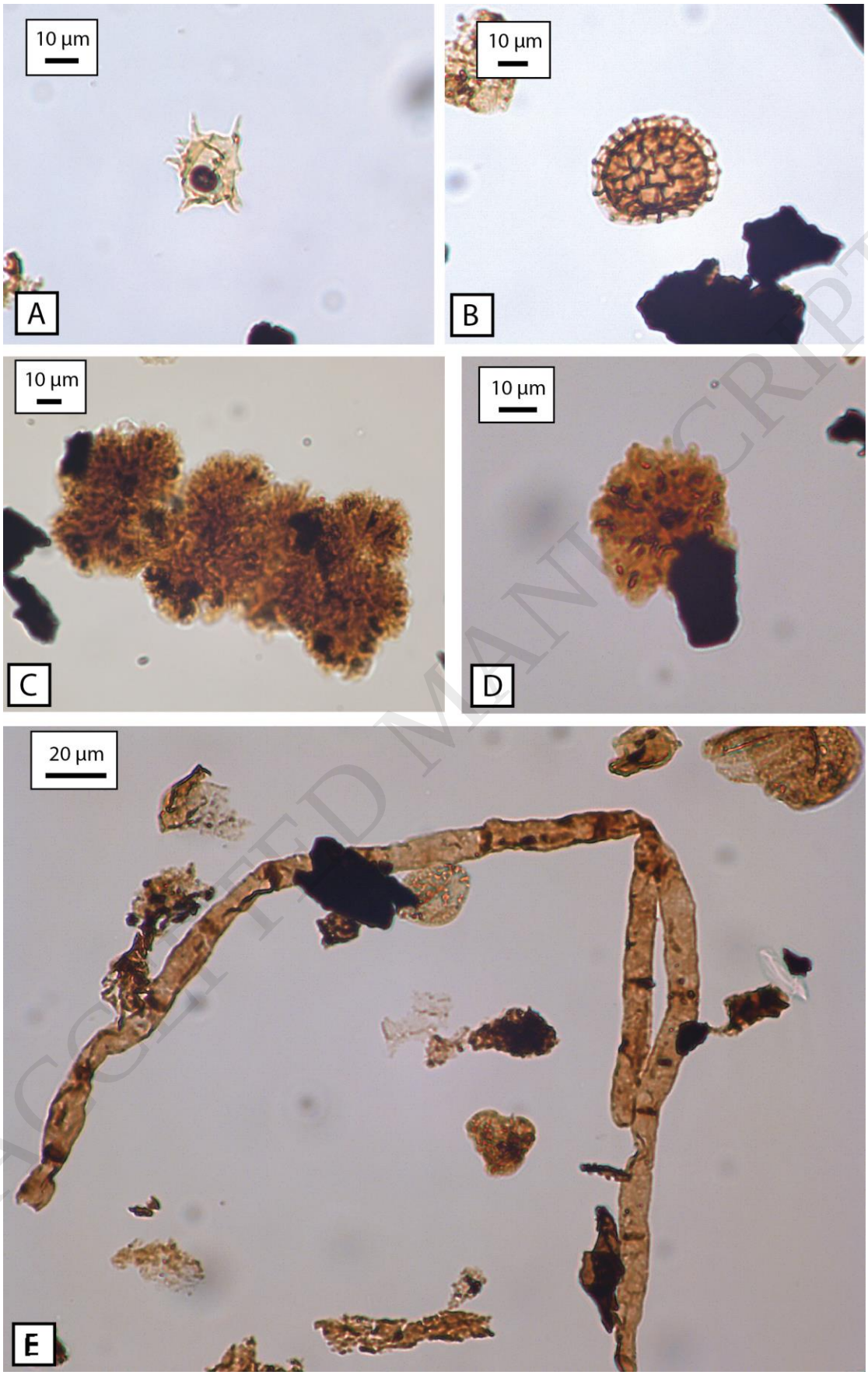

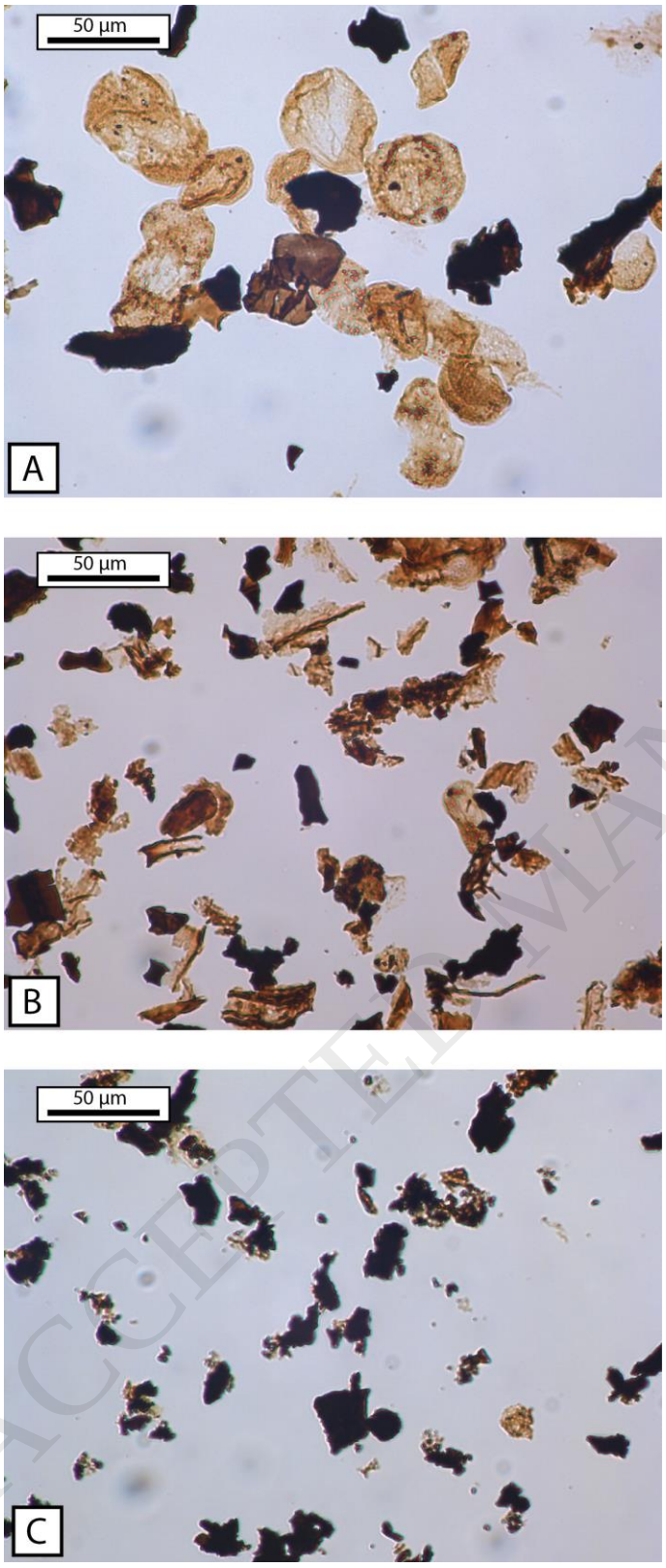

**Table:**

Table 1. Organic carbon isotope samples from GSQ Tambo 1-1A and their equivalent palynological samples.

| Sample name | Depth (m) | $\delta^{13}C$ (VPDB ‰) | Equivalent palynological sample |
|---|---|---|---|
| TAMI1 | 699.13 | -25.4 | TAMP5 |
| TAMI2 | 699.33 | -25.5 | TAMP6 |
| TAMI3 | 700.14 | -26.0 | TAMP7 |
| TAMI4 | 700.24 | -26.1 | TAMP8 |
| TAMI5 | 700.39 | -26.2 | TAMP9 |
| TAMI6 | 700.49 | -25.9 | TAMP10 |
| TAMI7 | 700.64 | -25.4 | TAMP11 |
| TAMI8 | 723.73 | -23.2 | TAMP13 |
| TAMI9 | 729.01 | -23.2 | TAMP14 |
| TAMI10 | 729.21 | -24.1 | TAMP15 |
| TAMI11 | 733.91 | -23.8 | TAMP16 |
| TAMI12 | 735.04 | -23.4 | TAMP17 |
| TAMI13 | 735.4 | -23.6 | TAMP18 |
| TAMI14 | 738.33 | -23.5 | TAMP19 |
| TAMI15 | 738.81 | -23.3 | TAMP20 |
| TAMI16 | 740.54 | -23.7 | TAMP21 |
| TAMI17 | 741.66 | -23.7 | TAMP22 |